

## Engineering polymers with improved charge transport properties from bithiophene-containing polyamides

Özen, Bilal; Candau, Nicolas; Temiz, Cansel; Grozema, Ferdinand C.; Fadaei Tirani, Farzaneh; Scopelliti, Rosario; Chenal, Jean Marc; Plummer, Christopher J.G.; Frauenrath, Holger

**DOI**

[10.1039/c9tc06544j](https://doi.org/10.1039/c9tc06544j)

**Publication date**

2020

**Document Version**

Accepted author manuscript

**Published in**

Journal of Materials Chemistry C

**Citation (APA)**

Özen, B., Candau, N., Temiz, C., Grozema, F. C., Fadaei Tirani, F., Scopelliti, R., Chenal, J. M., Plummer, C. J. G., & Frauenrath, H. (2020). Engineering polymers with improved charge transport properties from bithiophene-containing polyamides. *Journal of Materials Chemistry C*, *8*(18), 6281-6292. <https://doi.org/10.1039/c9tc06544j>

**Important note**

To cite this publication, please use the final published version (if applicable). Please check the document version above.

**Copyright**

Other than for strictly personal use, it is not permitted to download, forward or distribute the text or part of it, without the consent of the author(s) and/or copyright holder(s), unless the work is under an open content license such as Creative Commons.

**Takedown policy**

Please contact us and provide details if you believe this document breaches copyrights. We will remove access to the work immediately and investigate your claim.

# Engineering Polymers with Improved Charge Transport Properties from Bithiophene-Containing Polyamides

Bilal Özen,<sup>1</sup> Nicolas Candau,<sup>1</sup> Cansel Temiz,<sup>2</sup> Ferdinand C. Grozema,<sup>2</sup> Farzaneh Fadaei Tirani,<sup>3</sup>  
Rosario Scopelliti,<sup>3</sup> Jean-Marc Chenal,<sup>4</sup> Christopher J.G. Plummer,<sup>1</sup> Holger Frauenrath<sup>1,\*</sup>

<sup>1</sup> Ecole Polytechnique Fédérale de Lausanne (EPFL)  
Institute of Materials  
Laboratory of Macromolecular and Organic Materials

EPFL-STI-IMX-LMOM  
MXG 037, Station 12  
1015 Lausanne, Switzerland

<sup>2</sup> Delft University of Technology  
Department of Chemical Engineering

<sup>3</sup> Ecole Polytechnique Fédérale de Lausanne (EPFL)  
Institute of Chemical Science and Engineering

<sup>4</sup> University of Lyon, INSA de Lyon,  
MATEIS, CNRS, UMR 5510, 69621 Villeurbanne, France

\* Corresponding Author:  
holger.frauenrath@epfl.ch

## **Abstract**

Polymer semiconductors show unique combinations of mechanical and optoelectronic properties that strongly depend on their microstructure and morphology. Here, we have used a model  $\pi$ -conjugated bithiophene repeat unit to incorporate optoelectronic functionality into an aliphatic polyamide backbone by solution-phase polycondensation. Intermolecular hydrogen bonding between the amide groups ensured stable short-range order in the form of lamellar crystalline domains in the resulting semiaromatic polyamides, which could be processed from the melt and exhibited structural and thermomechanical characteristics comparable with those of existing engineering polyamides. At the same time, however, pulse-radiolysis time-resolved microwave conductivity measurements indicated charge carrier mobilities that were an order of magnitude greater than previously observed in bithiophene-based materials. Our results hence provide a convincing demonstration of the potential of amide hydrogen bonding interactions for obtaining unique combinations of mechanical and optoelectronic properties in thermoplastic polymers.

## Introduction

Polymer semiconductors are an important class of materials with charge transport behavior similar to conventional semiconductors, but which are inherently viscoelastic owing to their ability to form continuous elastic networks with a locally dissipative response, depending on the time scale of the measurement.<sup>1</sup> They may therefore show greatly enhanced strength and toughness compared with low molecular weight organic semiconductors.<sup>2</sup> However, they also show varying degrees of structural order, with important consequences for their macroscopic behavior. It is hence possible to tune the mechanical and optoelectronic properties of polymer semiconductors by controlling their structural order at different length scales.<sup>3-5</sup> This has led to a considerable effort over the last two decades to better understand the corresponding structure-property relationships, with the aim of designing and developing materials with increased charge carrier mobilities.<sup>6,7</sup> However, systematic investigations of the mechanical properties of polymer semiconductors are scarce and have largely focused on stretchable materials for wearable electronic devices, with little emphasis to date on high-performance engineering materials with useful electronic properties.<sup>8</sup>

Polymer semiconductors are typically semicrystalline, comprising amorphous regions and well-ordered crystalline domains characterized by two-dimensional lamellar stacks with a  $\pi$ -conjugated backbone, separated by layers of aliphatic side chains, as in the case of the prototypical regioregular poly(3-hexylthiophene).<sup>9,10</sup> The resulting morphology is complex, and understanding charge transport in such systems has consequently remained a challenge. However, recent studies have shown that efficient intermolecular charge transport may be achieved in high-performance polymer semiconductors that display high degrees of short-range order but no significant long range order and no phase boundaries, provided that aligned conjugated chain backbones form continuous paths between the locally ordered domains.<sup>3,11</sup>

Well-defined short-range order but limited long-range order are also characteristic features of many polyamides, which may exhibit lamellar crystalline domains with thicknesses of as little as 2 nm in the chain direction, corresponding to fewer than two repeat units, depending on their chemical structure.<sup>12,13</sup> These materials are highly sought after for engineering applications owing to their excellent specific mechanical strength, stiffness, and heat resistance, particularly when hydrogen bonding between the amide groups is combined with a partly or fully aromatic chain backbone.<sup>14,15</sup> We

have recently used transamidation during high-temperature melt compounding to introduce aliphatic substitutional defects into a high-performance semiaromatic copolyamide, with the aim of generating disorder in the crystalline lamellae while maintaining the degree of crystallinity and promoting strain-induced ordering in the amorphous regions, providing materials with improved toughness without compromising strength and stiffness.<sup>13,16</sup>

By contrast, the use of amide chemistry to control order and disorder at the nanoscale has seldom been investigated from the standpoint of organic electronics. Muguruma and coworkers prepared thin films from polyamides and polyurethanes containing quaterthiophene segments by co-deposition of appropriate difunctional monomers, but they did not provide details of the resulting structures nor the mechanical or electronic properties.<sup>17,18</sup> To the best of our knowledge, no other studies of the properties of polyamides containing organic semiconducting segments have so far been published. The effects of hydrogen bonding on the electronic properties of small molecules and polymers have nevertheless been extensively investigated both experimentally and through numerical modeling. It was originally supposed that hydrogen bonding might be detrimental to charge transport in organic semiconductors.<sup>19</sup> However, the subsequent emergence of small molecule and polymer semiconductors containing hydrogen bonds has shown this not to be the case. For instance, Glowacki *et al.* reported field-effect mobilities of up to  $1.5 \text{ cm}^2 \text{ V}^{-1} \text{ s}^{-1}$  in certain hydrogen-bonded heteroanalogues of pentacene and tetracene, and enhanced device lifetimes compared with those of their non-hydrogen bonded acene analogues.<sup>20</sup> Similarly, Würthner *et al.* found hydrogen-bonded octachloroperylene bisimide to be an efficient *n*-type semiconductor with field-effect mobilities of up to  $0.9 \text{ cm}^2 \text{ V}^{-1} \text{ s}^{-1}$ , and to show useful device lifetimes even under ambient conditions.<sup>21</sup> Moreover, recent computational studies of hydrogen-bonded *n*-type or *p*-type organic semiconductors have provided corroborating evidence of a beneficial effect of hydrogen bonding for electronic properties.<sup>22,23</sup> It follows that polyamide-based semiconductors may provide a means of combining outstanding mechanical performance with improved charge transport in a compositionally heterogeneous material, particularly if their local order can be tailored through a suitable choice of the molecular architecture and disposition of the functional groups.

Here, we demonstrate that hydrogen bonding associated with amide groups is indeed effective as a means of stabilizing the local packing of  $\pi$ -conjugated segments in a polymer. To this end, we have focused on the use of a bithiophene core as a model repeat unit to provide optoelectronic functionality.

Different polyamides were obtained by solution-phase polycondensation of a bithiophene dicarboxylic acid monomer with a range of aliphatic diamine monomers under Yamazaki-Higashi conditions. These materials were shown from extensive structural and thermomechanical analyses to reproduce many of the characteristics of typical engineering materials obtained from semiaromatic polyamides. At the same time, certain formulations showed significant charge carrier mobility, suggesting this to be a promising first step towards a functioning semiconducting engineering thermoplastic.

## Experimental Part

### *Materials and Instrumentation*

*Materials.* All materials and solvents were purchased from commercial suppliers and used without further purification. Chromatography solvents were purchased as reagent grades and distilled once prior to use. The progress of the reactions was monitored by thin-layer chromatography (TLC) on Merck TLC plates (Silica gel 60 F<sub>254</sub>). UV light (254 nm) was used for detection of compounds on the TLC plates. The detailed synthesis conditions for 3,3'-(2,2'-bithiophene-5,5'-diyl)dibutyric acid (**T2**) and dipropyl 4,4'-(2,2'-bithiophene-5,5'-diyl)dibutanamide (**T2a**) have been reported elsewhere.<sup>24</sup>

*NMR Spectroscopy.* NMR spectroscopy was performed on a Bruker Avance III 400 spectrometer at 400 MHz and 100 MHz magnetic field strength at 298 K for <sup>1</sup>H and <sup>13</sup>C nuclei, respectively. Deuterated solvents were purchased from Cambridge Isotope Laboratories, Inc. The spectra were calibrated to the respective residual solvent peaks of DMSO-*d*<sup>6</sup> (2.50 ppm <sup>1</sup>H NMR; 39.52 ppm <sup>13</sup>C NMR) or CDCl<sub>3</sub> (7.26 ppm <sup>1</sup>H NMR; 77.16 ppm <sup>13</sup>C NMR). The <sup>1</sup>H NMR spectra of the polyamides were recorded in non-deuterated 1,1,1,3,3,3-hexafluoropropan-2-ol with acetone-*d*<sup>6</sup> as the internal standard (2.05 ppm in <sup>1</sup>H NMR). Chemical shifts are expressed in parts per million (ppm) and coupling constants are given in Hz (s = singlet, d = doublet, t = triplet, q = quadruplet, p = quintet, m = multiplet, br = broad signal).

*Infrared Spectroscopy.* Infrared spectra were measured on a JASCO FT/IR 6300 spectrometer using the Miracle attenuated total reflection (ATR) accessory from PIKE.

*UV-vis Spectroscopy.* UV-vis spectra were measured on a Jasco V-670 spectrometer, solution phase spectra of 1,1,1,3,3,3-hexafluoropropane-2-ol (HFIP) solutions (5 mg/mL) were obtained using Hellma quartz cuvettes (1 mm path length), and spectra of thin films were measured on samples prepared onto a quartz substrate by spin-coating (4000 rpm, 1 min) using 100 μL of a stock solution (2 mg/mL).

*Mass Spectrometry.* High-resolution mass spectrometry was carried out on either a Waters Q-ToF Ultima for ESI or on a Waters QTOF Xevo G2-S for APPI.

*Single Crystal X-Ray Measurements.* Bragg-intensities were obtained from a single crystal of **T2a** at 200 K using a Rigaku SuperNova dual system diffractometer (CuK $\alpha$  radiation,  $\lambda = 1.54184 \text{ \AA}$ ) equipped with an Atlas S2 CCD detector. The dataset was reduced and corrected for absorption using CrysAlis<sup>Pro</sup>.<sup>25</sup> Solution and refinement of the crystal structures were performed using SHELXT<sup>26</sup> and SHELXL-2018<sup>27</sup>, respectively. All non-hydrogen atoms were refined anisotropically using the full-matrix least-squares method on  $|F|^2$ , while the hydrogen atoms were placed at calculated positions and refined using the riding model. Each H-atom was assigned a fixed isotropic displacement parameter with a value equal to 1.2  $U_{\text{eq}}$  of its parent C-atom (1.5  $U_{\text{eq}}$  for the methyl groups). The propyl-NH moiety was found to be disordered over two orientations found in a difference map and which were refined anisotropically using SADI and SIMU cards for the least-squares refinement, yielding site occupancies of 0.544(8)/0.456(8). Crystallographic and refinement data are summarized in Supplementary Tables S2–S3. The CCDC number 1951221 for compound **T2a** contains the supplementary crystallographic data for this paper. These data can be obtained free of charge via [www.ccdc.cam.ac.uk/data\\_request/cif](http://www.ccdc.cam.ac.uk/data_request/cif).

*X-Ray Diffraction and Structure Analysis.* 1D powder wide-angle X-Ray diffraction (WAXD) patterns for the as-synthesized polyamides were obtained in reflection mode using a PANalytical X'Pert Pro MPD diffractometer (CuK $\alpha$  radiation,  $\lambda = 1.54 \text{ \AA}$ ) in the Bragg-Brentano geometry. The X-ray tube was operated at 45 kV and 40 mA and scanning was carried out from  $2\theta = 15$  to  $30^\circ$  angles using a fixed divergence slit of  $0.25^\circ$ , a step size of  $0.0167^\circ$  and a time per step of 120.015 s.

Small-Angle X-ray Scattering (SAXS) patterns and 2D WAXD patterns for the recrystallized polyamides were obtained using a rotating anode X-Ray tube (CuK $\alpha$  radiation,  $\lambda = 1.54 \text{ \AA}$ ) at the MATEIS laboratory of the *Institut National des Sciences Appliquées* de Lyon, France. The data were recorded in transmission with a beam size of  $500 \mu\text{m} \times 500 \mu\text{m}$  and a 2D CCD detector (Princeton Instruments) with specimen-detector distances of 343 mm and 42.1 mm and exposure times of 180 and 1200 s for SAXS and WAXD respectively, corrected for the thickness and the absorption of the specimens, and integrated azimuthally. A broad low-angle peak observed in the SAXS patterns was assumed to arise from approximately periodic stacking of high aspect ratio crystalline lamellae, giving direct access to the lamellar long period,  $L_p$ . The lamellar thickness,  $L_c$ , was estimated from the corresponding

correlation function following Strobl and Schneider.<sup>28</sup> The volume fraction of the crystalline phase was then estimated from the ratio  $L_c / L_p$ .

Trial crystal structures for the polyamides were generated using the BIOVIA Materials Studio graphics user interface. Their geometry was then optimized with respect to all structural degrees of freedom subject to periodic boundary conditions, using classical force field-based energy minimization with the generic Dreiding force field<sup>29</sup> and the method of steepest descents with charge equilibration. WAXD patterns were simulated using the BIOVIA Reflex software package.

*Gel Permeation Chromatography (GPC).* The number and weight average molecular weights,  $M_n$  and  $M_w$ , and the dispersity,  $D$ , of the polyamides were determined using an Agilent 1260 Infinity GPC/SEC system with a refractive index detector and a total column length of 650 mm (PSS PFG, 100 Å). 1,1,1,3,3,3-hexafluoropropane-2-ol (HFIP) was used as the eluent at a flow rate of 1 mL/min and temperature of 25 °C. Six poly(methyl methacrylate) (PMMA) standards with molar masses of between 2'000 and 44'000 g/mol and  $D \leq 1.1$  were used for calibration. The polyamides and the PMMA standards were all dissolved in neat HFIP ( $c = 2$  mg/mL).

*Thermal Characterization.* Thermogravimetric analysis (TGA) scans were recorded using a Perkin Elmer TGA 4000. The specimens (5–10 mg) were dried in high vacuum at 80 °C for 24 h and then heated from 30 °C to 950 °C at a scanning rate of 10 °C/min in a flow of nitrogen (20 mL/min).

Differential scanning calorimetry (DSC) was carried out with a TA Instruments Q100 calorimeter at a scanning rate of 10°C/min under nitrogen flow (50 mL/min). Specimens of about 3–5 mg were first heated to a temperature 30 °C above their melting point and then cooled to 0 °C at a cooling rate of –10 °C/min in order to erase the effects of their thermal history. The data given for the thermal transitions were obtained from the second heating and first cooling scans. Melting ( $T_m$ ) and crystallization ( $T_c$ ) temperatures were defined as the temperatures corresponding to the maxima of the respective enthalpy peaks, while  $T_g$  was defined as the half-height of the heat capacity step associated with the glass transition. The melting enthalpies  $\Delta H_m$  were estimated by integrating the area under the melting peaks. The corresponding experimental errors are essentially due to the sensitivity of these measurements to the choice of baseline.

*Atomic Force Microscopy.* Pressed films with thicknesses of the order of 100  $\mu\text{m}$  were deposited on a flat glass substrate, heated to as temperature about 30 °C above their melting point as determined by DSC, and crystallized isothermally in air at the required temperature. The resulting surface textures

were observed by intermittent-contact-mode AFM (Bruker Nanoscope IIIa) with a MikroMasch NSC14 silicon probe (root-mean-square free amplitude = 2 V, set-point amplitude = 0.6–1.2 V).

*Polarized Optical Microscopy.* Polarized optical microscopy on the pressed films were carried out on an Olympus BH2 microscope equipped with Colorview I digital camera.

*Electron Microscopy.* Thin films of the polyamides for selected area electron diffraction (SAED) were obtained by friction deposition from a small block of the solid polyamide onto a freshly cleaved crystal of KBr held at 20–30 °C below the melting point of the polyamide, followed by dissolution of the KBr and deposition of the remaining oriented film onto a carbon covered 400 mesh grid. Electron fiber diffraction patterns were recorded using a Thermo Scientific Talos transmission electron microscope (TEM) operated at 200 kV.

*Nanoindentation Measurements.* Nanoindentation experiments were performed on 300  $\mu\text{m}$  thick pressed films of the polyamides, cooled at 10 °C/min from the melt, using an NHT<sup>2</sup> Nanoindentation Tester from Anton Paar equipped with a Berkovich diamond indenter ( $\alpha = 65.3 \pm 0.3$ ). Loading and unloading rates were set to 100 mN/min with a pause of 30 s, and the maximum load was 10 mN. 2–3 films were made from each material and a minimum of 25 indents were performed on two different areas of each. Hardness ( $H_{IT}$ ) and elastic modulus ( $E_{IT}$ ) were determined from the unloading part of the measurement using the method of Oliver and Pharr<sup>30</sup> and assuming a Poisson's ratio of 0.4 throughout.

*Dynamic Mechanical Analysis.* Dynamic mechanical testing (861<sup>e</sup>, Mettler Toledo) was performed in shear mode at room temperature with a strain amplitude of 0.1%. Each specimen was tested at successive frequencies of 10, 1 and 0.1 Hz. The test specimens were films of 0.3 mm in thickness with a geometric factor between 20–50  $\text{m}^{-1}$  prepared using a hot press under the same conditions as for the indentation measurements.

*Field-Effect Transistors.* Field-effect transistors were fabricated in two different configurations. The **PA6T2** polyamide solution (5 mg/mL in HFIP) was spin-coated (80  $\mu\text{L}$ , 4000 rpm) either onto heavily boron-doped silicon wafers ( $\text{Si}^+$ ) (525  $\mu\text{m}$ ) with a thermal oxide layer of 200 nm (capacitance,  $C = 19.5 \text{ nF/cm}^2$ ) that were purchased from the *Center of Micronanotechnology* at EPFL or onto Generation 4 Fraunhofer n-doped silicon microchips with 230 nm  $\text{SiO}_2$  gate dielectric ( $C = 18 \text{ nF/cm}^2$ ) with interdigitated gold source and drain electrodes (30 nm). For the former, top contacts were patterned via thermal deposition of gold source and drain electrodes (40 nm) in high vacuum (10-

6 mbar) through different shadow masks. Electrical characterizations of the field-effect transistors were performed under the inert atmosphere of a glovebox with a Keithley 4200 parameter analyzer.

*Pulse Radiolysis Time-Resolved Microwave Conductivity.* Charges were generated in powder samples (20–50 mg) by irradiation with short pulses (2–20 ns) of high-energy electrons (3 MeV) from a Van de Graaff accelerator. The penetration depth of these high-energy electrons in the materials is several millimeters, resulting in close to homogenous ionization and hence a uniform concentration of charges. The change in conductivity of the material due to charges generated by the irradiation was probed using high frequency microwaves (28 to 38 GHz). The fractional change in the microwave power ( $\Delta P/P$ ) absorbed on irradiation is directly proportional to the change in the conductivity ( $\Delta\sigma$ ) according to

$$\frac{\Delta P}{P} = -A\Delta\sigma$$

where the sensitivity factor,  $A$ , is a sensitivity factor that depends on the geometric and dielectric properties of the material.<sup>31</sup> The conductivity ( $\Delta\sigma$ ) is related to the mobility of all charged species, and their concentration,  $N_p$ , through

$$\Delta\sigma = eN_p \sum \mu$$

where  $e$  is the elementary charge ( $1.6 \cdot 10^{-19}$  C). This this is equation allows the mobility of the charge carriers to be calculated given a reasonable estimate of their concentration. Such an estimate may be obtained from dosimetry measurements, which provides the amount of energy deposited by the electron pulse, as described in detail previously.<sup>32</sup>

#### *Synthesis Procedures and Analytical Data*

**General Procedure for the Synthesis of Semiaromatic Polyamides (PAnT2).** A flame-dried 50 mL Schlenk tube equipped with a stirring bar was charged with the aliphatic diamine (0.50–3.00 mmol), bithiophene dibutyric acid **T2** (1.00 eq.), a mixture of anhydrous *N*-methylpyrrolidone (NMP) and anhydrous pyridine (4:1, 3–11 mL), triphenylphosphite (TPP) (2.01 equiv.), as well as anhydrous lithium chloride (LiCl) (4 wt%) in a flow of argon. The suspension was heated to 120 °C under vigorous stirring. After 4 h, the solution was poured into MeOH (250 mL). The resulting precipitate was filtered off, washed several times with hot MeOH, and dried in vacuum to yield the desired polyamide **PAnT2** as a yellow powder.

**Poly(hexamethylene bithiophenedibutanamide) (PA6T2).** The general procedure for the synthesis of semiaromatic polyamides was followed, starting from 1,6-hexanediamine (316 mg,

2.72 mmol) and bithiophene dibutyric acid **T2** (2.72 mmol), to give the desired polyamide **PA6T2** in a yield of 1.04 g (90%) after precipitation.  $^1\text{H}$  NMR (400 MHz, acetone- $d_6$ ):  $\delta$  = 6.10 (s, 2H), 5.83 (s, 2H), 5.26 (br, 2H), 2.33 (q,  $J$  = 6.1, 5.6 Hz, 4H), 1.93 (t,  $J$  = 6.0 Hz, 4H), 1.43–1.33 (m, 4H), 1.16–0.98 (m, 4H), 0.63 (br, 4H), 0.45 (br, 4H) ppm. GPC (HFIP):  $M_n$  = 13'500 ( $\mathcal{D}$  = 1.5).

**Poly(heptamethylene bithiophenedibutanamide) (PA7T2).** The general procedure for the synthesis of semiaromatic polyamides was followed, starting from 1,7-heptanediamine (100 mg, 0.77 mmol) and bithiophene dibutyric acid **T2** (0.77 mmol), to give the desired polyamide **PA7T2** in a yield of 270 mg (88%) after precipitation.  $^1\text{H}$  NMR (400 MHz, acetone- $d_6$ ):  $\delta$  = 6.10 (s, 2H), 5.84 (s, 2H), 5.22 (br, 2H), 2.34 (dd,  $J$  = 12.1, 6.2 Hz, 3H), 1.94 (t,  $J$  = 7.3 Hz, 3H), 1.39 (t,  $J$  = 7.3 Hz, 2H), 1.14 – 1.03 (m, 2H), 0.63 (br, 2H), 0.45 (br, 4H) ppm. GPC (HFIP):  $M_n$  = 12'500 ( $\mathcal{D}$  = 1.6).

**Poly(octamethylene bithiophenedibutanamide) (PA8T2).** The general procedure was followed for the synthesis of semiaromatic polyamides, starting from 1,8-octanediamine (282 mg, 1.96 mmol) and bithiophene dibutyric acid **T2** (1.96 mmol), to give the desired polyamide **PA8T2** in a yield of 810 mg (90%) after precipitation.  $^1\text{H}$  NMR (400 MHz, acetone- $d_6$ ):  $\delta$  = 6.10 (d,  $J$  = 1.9 Hz, 2H), 5.84 (s, 2H), 2.33 (dd,  $J$  = 12.7, 7.3 Hz, 4H), 1.94 (t,  $J$  = 7.0 Hz, 4H), 1.39 (t,  $J$  = 7.5 Hz, 4H), 1.14 – 1.03 (m, 4H), 0.63 (br, 2H), 0.44 (br, 8H) ppm. GPC (HFIP):  $M_n$  = 12'700 ( $\mathcal{D}$  = 1.5).

**Poly(nonamethylene bithiophenedibutanamide) (PA9T2).** The general procedure for the synthesis of semiaromatic polyamides was followed, starting from 1,9-nonanediamine (146 mg, 0.92 mmol) and bithiophene dibutyric acid **T2** (0.92 mmol), to give the desired polyamide **PA9T2** in a yield of 390 mg (88%) after precipitation.  $^1\text{H}$  NMR (400 MHz, acetone- $d_6$ ):  $\delta$  = 6.10 (d,  $J$  = 2.7 Hz, 2H), 5.84 (s, 2H), 5.20 (br, 2H), 2.33 (dd,  $J$  = 11.5, 5.4 Hz, 4H), 1.95 (t,  $J$  = 5.4 Hz, 4H), 1.39 (t,  $J$  = 7.7 Hz, 4H), 1.14 – 1.03 (m, 4H), 0.62 (br, 4H), 0.43 (br, 10H) ppm. GPC (HFIP):  $M_n$  = 10'600 ( $\mathcal{D}$  = 2).

**Poly(decamethylene bithiophenedibutanamide) (PA10T2).** The general procedure for the synthesis of semiaromatic polyamides was followed, starting from 1,10-decanediamine (146 mg, 0.85 mmol) and bithiophene dibutyric acid **T2** (0.85 mmol), to give the desired polyamide **PA10T2** in a yield of 380 mg (91%) after precipitation.  $^1\text{H}$  NMR (400 MHz, acetone- $d_6$ ):  $\delta$  = 6.08 (d,  $J$  = 2.3 Hz, 2H), 5.81 (d,  $J$  = 2.1 Hz, 2H), 5.17 (br, 2H), 2.30 (d,  $J$  = 6.0 Hz, 4H), 1.92 (t,  $J$  = 6.6 Hz, 4H), 1.36 (t,  $J$  = 7.2 Hz, 4H), 1.15 – 0.97 (m, 4H), 0.59 (br, 4H), 0.40 (br, 12H) ppm. GPC (HFIP):  $M_n$  = 10'300 ( $\mathcal{D}$  = 2).

**Poly(undecamethylene bithiophenedibutanamide) (PA11T2).** The general procedure was followed for the synthesis of semiaromatic polyamides, starting from 1,11-undecanediamine (120 mg, 0.64 mmol) and bithiophene dibutyric acid **T2** (0.64 mmol), to give the desired polyamide **PA11T2** in

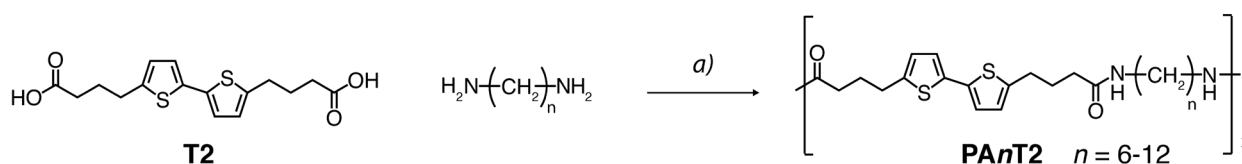
a yield of 300 mg (86%) after precipitation.  $^1\text{H NMR}$  (400 MHz, acetone- $d_6$ ):  $\delta$  = 6.14–6.06 (m, 2H), 5.84 (s, 2H), 5.20 (br, 2H), 2.32 (dd,  $J$  = 11.4, 5.2 Hz, 4H), 2.02–1.88 (m, 4H), 1.48–1.30 (m, 4H), 1.15–1.02 (m, 4H), 0.61 (br, 4H), 0.42 (br, 14H) ppm. GPC (HFIP):  $M_n$  = 8'600 ( $\mathcal{D}$  = 1.9).

**Poly(dodecamethylene bithiophenedibutanamide) (PA12T2).** The general procedure for the synthesis of semiaromatic polyamides was followed, starting from 1,12-dodecanediamine (142 mg, 0.71 mmol) and bithiophene dibutyric acid **T2** (0.71 mmol), to give the desired polyamide **PA12T2** in a yield of 330 mg (89%) after precipitation.  $^1\text{H NMR}$  (400 MHz, acetone- $d_6$ ):  $\delta$  = 6.07 (d,  $J$  = 2.2 Hz, 2H), 5.81 (s, 2H), 5.16 (s, 2H), 2.30 (d,  $J$  = 5.9 Hz, 4H), 1.92 (s, 4H), 1.36 (t,  $J$  = 7.0 Hz, 4H), 1.14 – 0.95 (m, 4H), 0.59 (br, 4H), 0.39 (br, 16H) ppm. GPC (HFIP):  $M_n$  = 10'700 ( $\mathcal{D}$  = 1.9).

## Results and Discussion

### Synthesis of Bithiophene-Containing Semiaromatic Polyamides

We prepared a series of polyamides **PAnT2** by solution-phase polycondensation of bithiophene dibutyric acid **T2** with different aliphatic diamines (with  $n$  carbon atoms) under standard Yamazaki-Higashi conditions<sup>33–35</sup>, that is, using triphenylphosphite (TPP) and LiCl in a mixture of anhydrous NMP and pyridine (Scheme 1, Table 1). Successful conversion was proven by 1D and 2D NMR as well as solid-state IR spectroscopy (Supplementary Figure S1, Figure 2). Gel permeation chromatography (GPC) in HFIP indicated number average molar masses ( $M_n$ ) on the order of 8'600–13'000 g/mol and dispersities ( $\mathcal{D}$ ) of 1.5–2.0 (Table 1). The polymers were soluble in 1,1,1,3,3,3-hexa-fluoropropan-2-ol (HFIP) at room temperature and in polar solvents such as hexamethylphosphoramide (HMPA), *m*-cresol, dimethylacetamide upon heating, but insoluble in dimethyl sulfoxide (DMSO), dimethylformamide (DMF), *N*-methyl-2-pyrrolidone (NMP), 1,2-dichlorobenzene, glacial acetic acid, xylenes, cyclohexanone, or chlorobenzene even at elevated temperatures.



**Scheme 1.** Synthesis of semiaromatic polyamides **PAnT2** by solution-phase polycondensation using Yamazaki-Higashi conditions. *Reaction conditions:* a) triphenylphosphite (TPP), LiCl, NMP/pyridine (4:1), 120 °C, 4h, 86–91%.

**Table 1.** Yields, molecular weights, and dispersities (from gel permeation chromatography) of **PAnT2**.

Polyamide				GPC		
<b>PAnT2</b>	<i>n</i>	Amount [g]	Yield [%]	$M_n$ [g/mol]	$M_w$ [g/mol]	$\bar{D}$
<b>PA6T2</b>	6	1.04	90	13'500	20'100	1.5
<b>PA7T2</b>	7	0.27	88	12'500	20'100	1.6
<b>PA8T2</b>	8	0.81	90	12'700	19'400	1.5
<b>PA9T2</b>	9	0.39	88	10'600	20'800	2.0
<b>PA10T2</b>	10	0.38	91	10'300	20'300	2.0
<b>PA11T2</b>	11	0.30	86	8'600	16'100	1.9
<b>PA12T2</b>	12	0.33	89	10'700	20'600	1.9

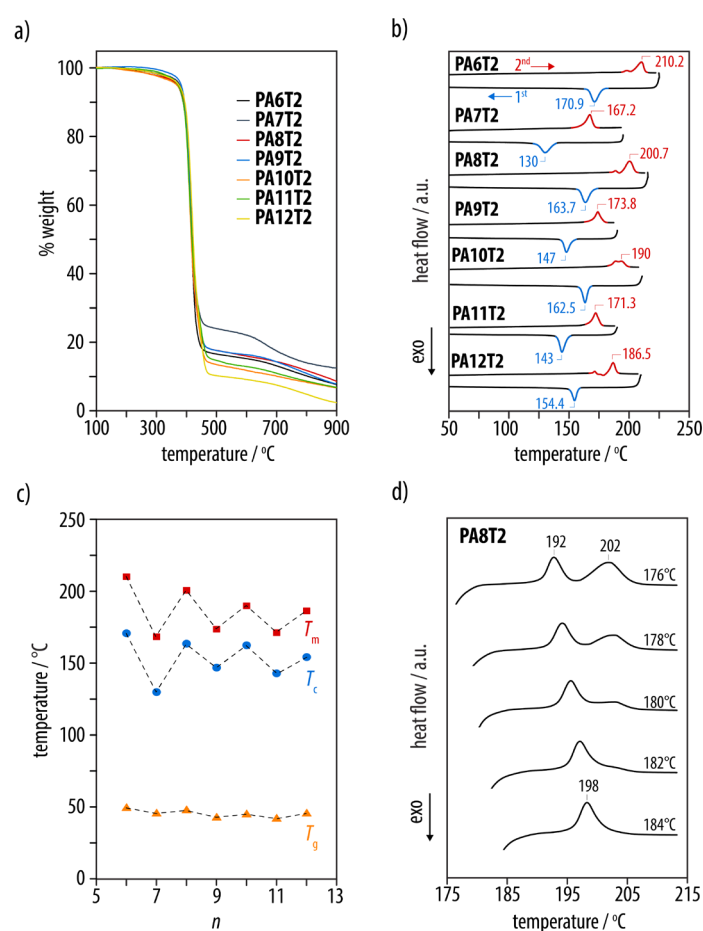


**Figure 1.** a) Results from thermogravimetric analysis (TGA) scans of **PAnT2** indicated a main decomposition temperature above 300 °C. b) Successive dynamic scanning calorimetry (DSC) cooling and heating scans from **PAnT2** ( $n = 6$  to 12) at 10 °C/min. Melting of **PAnT2** with even  $n$  was characterized by multiple melting endotherms, whereas only a single endotherm was observed for odd  $n$ . c) The corresponding melting and crystallization temperatures showed a global decrease with increasing  $n$  but were reduced for odd  $n$  with respect to the values obtained for adjacent even  $n$ . d) Representative examples of DSC heating scans at 10 °C/min from **PA8T2** after isothermal crystallization from the melt at the specified temperatures.

Thermogravimetric analysis (TGA) measurements on **PAnT2** indicated a mass loss of 1–2% at about 250 °C, marking the onset of decomposition, and more substantial mass loss above 300 °C (Figure 1a). Differential scanning calorimetry (DSC) scans were hence performed in the temperature range below 250 °C to minimize thermal degradation effects. All polymers **PAnT2** were semicrystalline according to DSC heating scans at 10 °C/min but showed distinct melting and crystallization behavior depending on  $n$  (Figure 1b,c). The highest melting and crystallization temperatures of 210 and 171 °C, respectively, were observed for **PA6T2**. However, although the main melting and crystallization temperatures showed a global decrease with increasing  $n$ , there was also a clear odd/even effect, with odd  $n$  resulting in significantly lower transition temperatures than adjacent even  $n$  (Figure 1c), as reported previously for other polyamides, such as the series **PAn10** ( $n = 6$  to 12).<sup>36</sup> By contrast, the **PAnT2** glass transition temperature ( $T_g$ ) measured from the heating scans showed only a weak global decrease with increasing  $n$  with a correspondingly slight odd-even effect (Figure 1c).

The crystalline structures of polyamides **PAnT2** are expected to follow the trends typical of other dyadic aliphatic polyamides. Optimum hydrogen bonding between parallel chains in the all-*trans* conformation is only possible in even-even polyamides that are therefore able to adopt the triclinic  $\alpha$ -type crystalline form, consisting of stacks of planar hydrogen bonded sheets of fully extended chains.<sup>14,36,37</sup> By contrast, even-odd, odd-even and odd-odd polyamides typically form pseudo-hexagonal pleated sheet structures, collectively referred to as the  $\gamma$  phase, in which the plane of the amide groups tilts away from that of the methylene groups to allow formation of intersheet hydrogen bonds.<sup>38</sup> Because the **T2** repeat units are effectively “even” repeat units, the stability of crystalline **PAnT2** as reflected by the melting point should be significantly higher for even  $n$  than for odd  $n$ , as observed here. **PAnT2** with odd  $n$  also showed a single melting endotherm in DSC heating scans at 10 °C/min, whereas at least two endotherms were observed for **PAnT2** with even  $n$ . The separation of these endotherms was most marked after isothermal crystallization at comparatively low temperatures, suggesting the odd/even effect to influence the recrystallization or reorganization behavior of the crystalline phase (Figure 1d, Supplementary Figure S2).<sup>39</sup>

### *Structural Characterization*

Solid-state infrared (IR) spectra of the polyamides **PAnT2** (Figure 2a,b) with  $n = 6$ –10 showed that the broad absorption at 2700–3300  $\text{cm}^{-1}$  and the band at 1688  $\text{cm}^{-1}$  associated with the O–H and C=O stretching vibrations of the free carboxylic acid group of the **T2** monomer to be replaced by the

characteristic amide A ( $3304\text{ cm}^{-1}$ , FWHM  $82\text{ cm}^{-1}$ , N–H stretching), amide I ( $1634\text{ cm}^{-1}$ , FWHM  $32\text{ cm}^{-1}$ , C=O stretching), and amide II ( $1534\text{ cm}^{-1}$ , C=O bending), consistent with typical IR spectral features in semicrystalline polyamides (Supplementary Table S1).<sup>40</sup> Because the same N–H and C=O stretching vibrations were observed in specimens of the bithiophene dipropylamide model compound **T2a**, whose of which the crystal structure was known (see below), one may infer from the IR spectra that the polymers **PAnT2** comprised polymer chains organized into hydrogen-bonded sheets. The same principal absorptions were also observed for the polyamides **PAnT2** (Figure 2*a,b*) with  $n = 11\text{--}12$ , but their amide A and amide II absorptions were significantly broadened, indicating a lower degree of order.

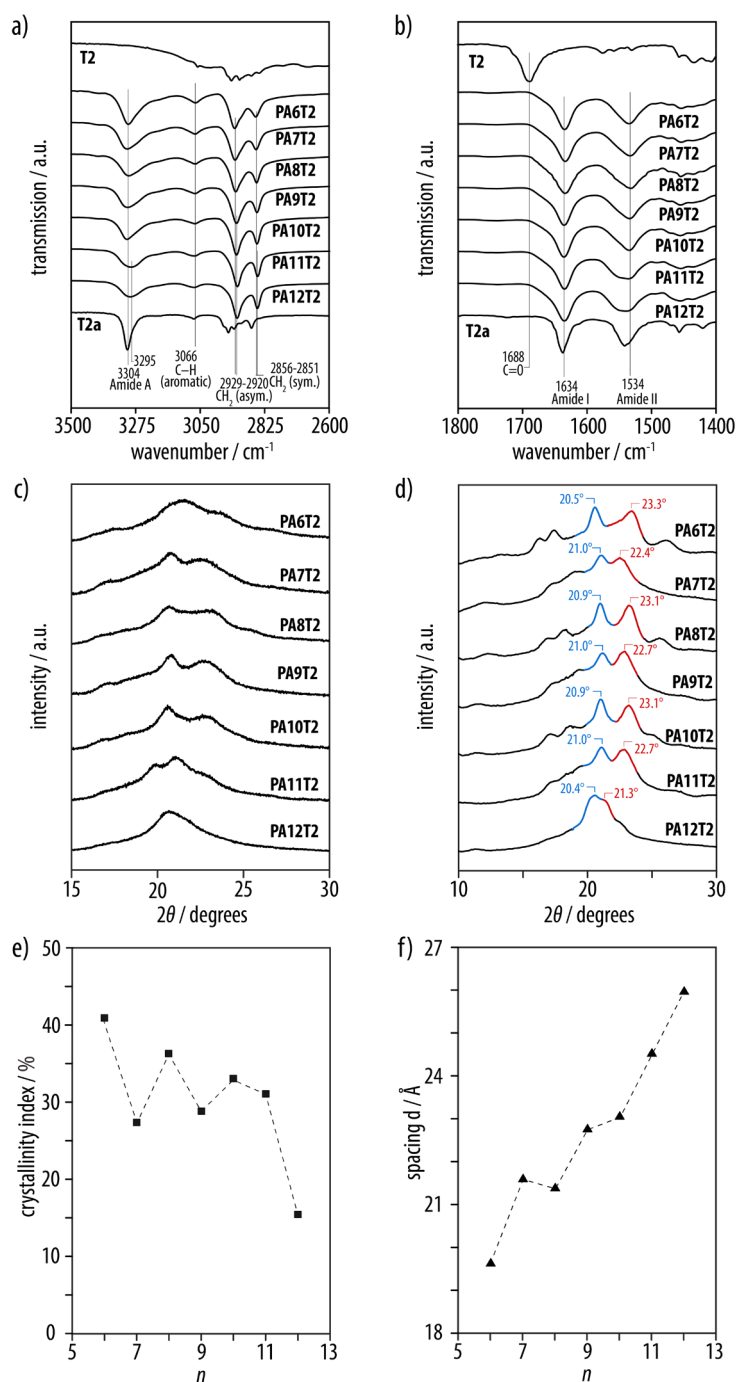


**Figure 2.** *a,b*) Solid-state IR spectra of the bithiophene dibutyric acid **T2**, model compound **T2a** and the resulting polyamides **PA $n$ T2**. After polycondensation, the C=O stretching vibration of the free carboxylic acid was replaced by the amide A, I, and II bands of the amide functions. *c*) Wide-angle X-Ray diffraction (WAXD) patterns from the as-synthesized (powder) and *d*) isothermally crystallized (bulk) specimens recorded at room temperature in reflection and transmission, respectively. *e*) Degree of crystallinity for **PA $n$ T2** estimated from deconvolution of the WAXD profiles (Supplementary Figure S3). *f*) Spacings corresponding to the lowest angle Bragg reflections from the WAXD patterns of the melt-crystallized polyamides shown as a function of  $n$ .

WAXD patterns confirmed the presence of an ordered phase in the as-synthesized **PA $n$ T2** (Figure 2c), and sharp well-defined Bragg peaks were visible after isothermal crystallization at a temperature

10 °C higher than the temperature of the crystallization peak in the cooling scans (Figure 2d). Consistent with the DSC results and IR spectra, the degree of crystallinity estimated from the WAXD patterns (Figure 2e, Supplementary Figure S3) showed a global decrease with  $n$ , and again some suggestion of an odd/even effect at low  $n$ , although it fell off sharply for  $n = 12$ .

For  $n < 12$ , strong, well-separated reflections were observed at  $2\theta = 22.4\text{--}23.3^\circ$  and  $2\theta = 20.4\text{--}21^\circ$ , corresponding to  $d$ -spacings in the range 3.80–3.97 and 4.23–4.35 Å, respectively, while for  $n = 12$ , the main peaks overlapped. Prominent low-angle peaks corresponding to  $d$ -spacings in the range of 19–26 Å were also present (Figure 2f). The  $d$  spacings corresponding to the low angle WAXD peaks for **PAnT2** with odd  $n$  were greater than expected from interpolation of the data for even  $n$  (Figure 2f), suggesting the  $c$  axis of the unit cell to lie closer to the basal plane normal for odd  $n$ . As discussed above, if  $n$  is odd, optimum hydrogen bonding is no longer possible with the aliphatic sub-chains in the all-*trans* conformation. Hence, by analogy with aliphatic polyamides with odd  $n$ , such as PA56, consecutive amide groups along the chain may tilt in opposite directions away from the plane of the methyl groups to form hydrogen bonds, leading to more compact conformations and a reduction in the  $c$ -repeat distance. The required tilt of the amide groups is nevertheless small, resulting in monoclinic packing and a centered unit cell in which the overall chain conformations remain close to the all-*trans* conformations characteristic of the  $\alpha$  phase.<sup>41</sup>

To model the molecular arrangement of the polyamides **PAnT2**, and specifically the packing behavior of the bithiophene unit, we used the single-crystal X-ray structure of model compound **T2a** as a starting point,<sup>24</sup> because its solid-state IR spectra showed very similar features (Figure 2a,b). **T2a** crystallized in the triclinic space group  $P1\bar{1}$  with the lattice parameters  $a = 4.9848(4)$  Å,  $b = 5.6250(5)$  Å,  $c = 21.347(3)$  Å,  $\alpha = 90.584(9)^\circ$ ,  $\beta = 90.140(8)^\circ$ , and  $\gamma = 107.702(8)^\circ$  and a single molecule in the unit cell (Figure 3, Supplementary Tables S2–S3). The amide functions formed two infinite arrays of almost linear intermolecular N–H $\cdots$ O=C hydrogen bonds (N–H $\cdots$ O  $\sphericalangle$  162°, H $\cdots$ O  $d = 2.02$  Å) with opposite orientation along the crystallographic  $a$ -axis. Simultaneously, the bithiophenes adopted a parallel-displaced  $\pi$ -stacked arrangement with an interlayer spacing of 3.6 Å, a tilt angle of 40.5° relative to the crystallographic  $c$ -direction, and various intermolecular C $\cdots$ C, C $\cdots$ S, and S $\cdots$ S close contacts (Figure 3c,d).

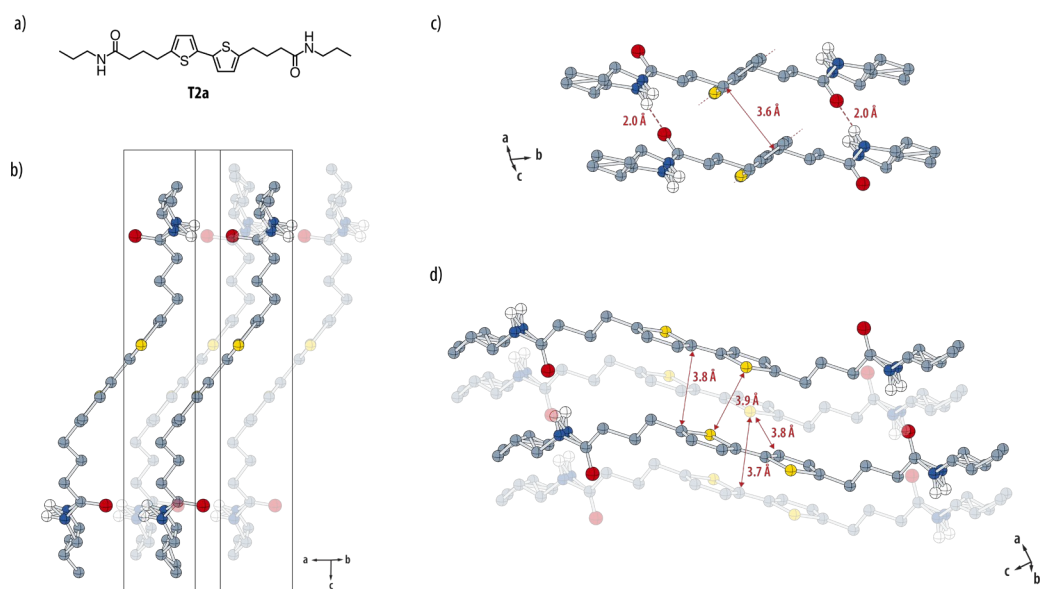


**Figure 3.** *a)* Molecular structure of the bithiophene diamide model compound **T2a**. *b)* Ball-and-stick representations of the single-crystal X-ray structure of **T2a** viewed along the *ab*-plane, showing the presence of both N-H  $\cdots$  O=C hydrogen bonds and the parallel-displaced  $\pi$ -stacked arrangement of the bithiophene units with *c)* a hydrogen bonding distance (H $\cdots$ O) of 2.0 Å and a bithiophene interlayer distance of 3.6 Å. *d)* C $\cdots$ S and C $\cdots$ C and S $\cdots$ S close contacts between parallel-displaced pairs of bithiophenes (all hydrogen atoms except those that participate in hydrogen bonding have been omitted for clarity).

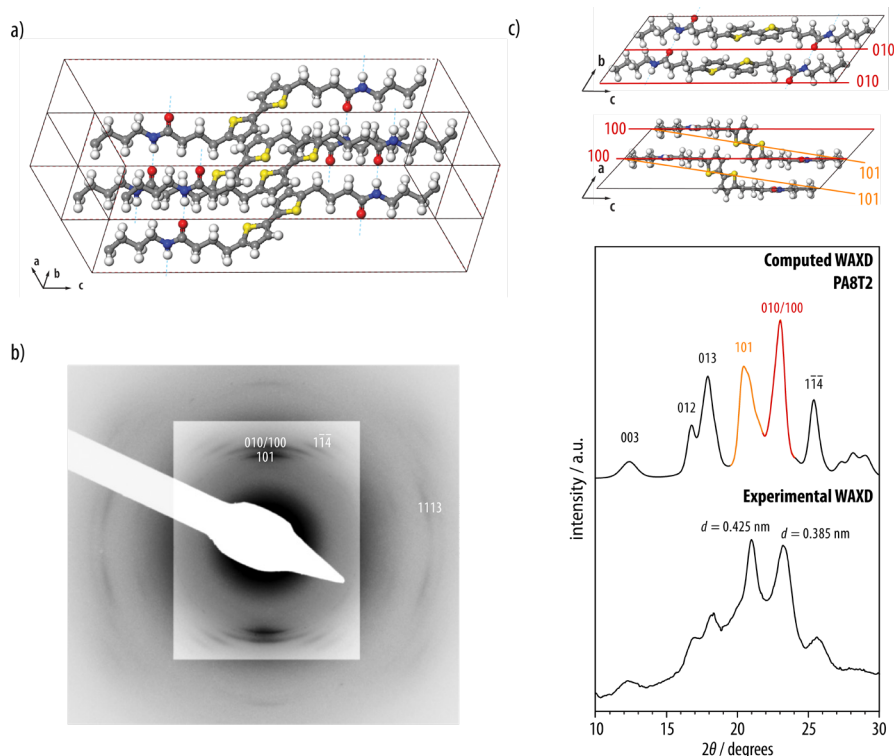


**Figure 4.** *a)* Model structure for **PAnT2** with even  $n$ , shown here for  $n = 8$ , assuming a triclinic  $P\bar{1}$  space group with the  $c$  axis parallel to the axes of the main methyl sub-chain. *b)* Selected area electron diffraction (SAED) pattern from an oriented film of **PAnT2**. *c)* Comparison of the experimental WAXD data for a melt crystallized film of **PAnT2** with a simulated WAXD powder pattern from the structure in *a)* with lattice parameters  $a = 5.10$  Å,  $b = 5.68$  Å,  $c = 30.61$  Å,  $\alpha = 60.40^\circ$ ,  $\beta = 71.24^\circ$ ,  $\gamma = 109.68^\circ$  derived from the SAED pattern.

Trial crystal structures for **PA $n$ T2** with even  $n$  (Figure 4a) were hence generated assuming a triclinic unit cell, packing and conformations analogous to those observed for **T2a**, and an all-*trans* conformation for the aliphatic segments, consistent with the solid-state IR spectra. For convenience, the  $c$  axis of the unit cell was chosen to be parallel to the axis of the aliphatic sub-chains, so that changes in  $n$  could be accommodated by adjusting  $c$ . In the case of  $n = 8$ , the unit cell parameters were adjusted to fit the peak positions from selected-area electron diffraction (SAED) patterns from oriented friction deposited films (Figure 4b), in which the higher order peaks were well resolved and the layer line spacing provided an estimate of the  $c$  repeat distance along the orientation axis. The energy was then minimized, resulting in a hydrogen bond distance (H...O) of 2.0 Å, as observed for the model compound **T2a**. Simulated WAXD powder patterns based on this structure, with crystal dimensions of 150 Å in the  $a$  and  $b$  directions and 50 Å in the  $c$  direction, were in satisfactory agreement with the experimental WAXD data from **PA8T2** isothermally crystallized from the melt at 175 °C (Figure 4c). The peak at  $2\theta$  of around 23° in **PA6T2**, **PA8T2**, and **PA10T2** was hence identified with scattering from the (100) and (010) planes, whereas the peak at  $2\theta$  of 20.5 to 20.9° was dominated by contributions from the (101) planes. Hence, in contrast to the  $\alpha$  phase of PA66<sup>42</sup> and its homologues, there was little scattering from the planes perpendicular to the hydrogen bond direction, because the alignment of the sheets formed locally by the hydrogen-bonded aliphatic chains was interrupted by the bithiophene units.

SAXS data for **PA $n$ T2** with even  $n$  crystallized under the same conditions as for the WAXD measurements suggested lamellar thicknesses,  $L_c$ , that decreased from about 40 Å in **PA6T2** and **PA8T2** to 22 Å in **PA10T2** and **PA12T2**, assuming a two-phase lamellar structure (Figure 5a,b). Hence, the  $L_c$  for **PA6T2** and **PA8T2** were about 2.0  $d_{001}$  and 1.9  $d_{001}$ , respectively, while for **PA10T2** and **PA12T2**,  $L_c$  and  $d_{001}$  were roughly equal. For comparison, lamellar thicknesses of as little as 20 Å have been reported for rapidly cooled aliphatic and semiaromatic polyamides.<sup>12</sup> The lamellar spacing,  $L_p$ , determined by SAXS remained close to 110 Å for all polyamides **PA $n$ T2**. The corresponding SAXS degree of crystallinity was therefore about 35 vol% for  $n = 6$  and 8 but decreased to about 20 vol% at higher  $n$  (Figure 5c), consistent with the values obtained from WAXD. This compares with typical values of 30 vol% for semiaromatic polyamides<sup>43,44</sup> with comparable aliphatic sequence lengths.

Images obtained by AFM of films of **PA8T2** on glass substrates melt-crystallized at 176 °C in air indicated a two-dimensional banded spherulitic texture and a minimum lamellar spacing, corresponding to edge-on lamellae, of 100–140 Å in thickness (Figure 5e, Supplementary Figure S4), in

good agreement with the SAXS data for  $L_p$ . As the rigid bithiophene unit cannot easily accommodate chain folding, we conclude that the crystalline lamellar structure in melt-crystallized **PA $n$ T2** (with even  $n$  from 6 to 10) consisted of two layers of parallel-displaced,  $\pi$ -stacked bithiophenes separated by a layer of inclined hydrogen-bonded aliphatic chains in the all-*trans* conformation (Figure 5d). In the case of **PA $n$ T2** with odd  $n$ , when melt-crystallized under quiescent conditions, the corresponding SAED results indicated more limited three-dimensional order (Supplementary Figure S5), in agreement with the observations from DSC and WAXD.

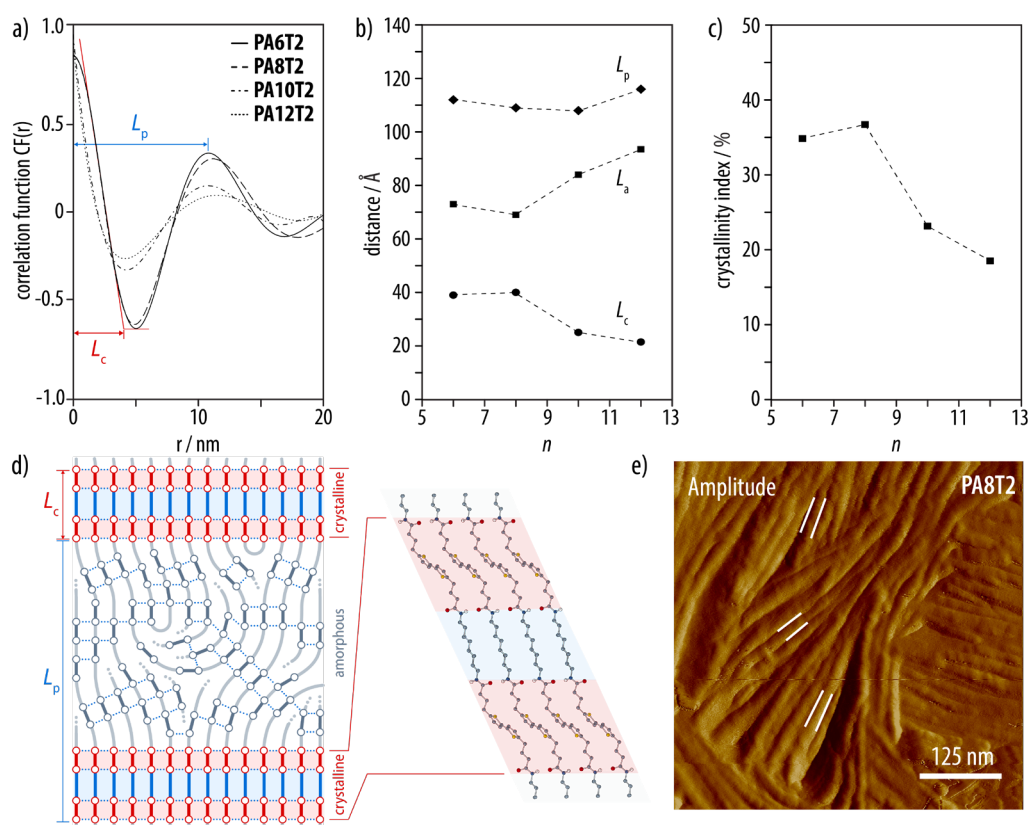


**Figure 5.** a) Estimation of the lamellar thickness ( $L_c$ ) and lamellar long period ( $L_p$ ) from the small-angle X-Ray scattering (SAXS) correlation function for even  $n$ , assuming a two-phase model. b) Estimated  $L_c$  and  $L_p$  for the even polyamides along with  $L_a$ , the thickness of the corresponding amorphous layer, taken to be equal to  $L_p - L_c$ . c) Degree of crystallinity for **PA $n$ T2** estimated from the SAXS measurements (even  $n$  only). d) Schematic representation of the lamellar morphology of **PA8T2**. e) Atomic force microscopy (AFM) intermittent contact mode height image the local lamellar structure in a film of **PA8T2** isothermally crystallized from the melt at 176 °C. The white markers are separated by 10 nm. See Supplementary Figure S4 for more information.

### Mechanical Characterization

Nanoindentation and dynamic mechanical analysis (DMA) measurements were used to evaluate the mechanical properties of polyamide **PA $n$ T2** films compression molded at their nominal melting

temperature and subsequently cooled at 10 °C/min (Figure 6a). A peak at about 210 MPa was observed in the mean instrumented hardness from the nanoindentation measurements,  $H_{IT}$ , for  $n = 7$ , and then a gradual decrease with increasing  $n$  (Figure 6b), consistent with the evolution of the melting enthalpy of the films measured by DSC (Figure 6d). The absolute values of  $H_{IT}$  were hence similar to the value of 176 MPa obtained from the aliphatic polyamide PA610 ( $H_{IT} = 176$  MPa), but lower than the value of 404 MPa obtained from the industrial-grade semiaromatic polyamide poly(hexamethylene terephthalamide-*co*-isophthalamide) (PA6TI) (Supplementary Figure S6). Elastic moduli,  $E_{IT}$ , close to 2.9 GPa were obtained for  $n = 6$  and 7 from the unloading curves (Figure 6a, Supplementary Figure S6) according to the method of Oliver and Pharr, as compared to 3.8 MPa for PA6TI.  $E_{IT}$  then decreased gradually from 2.5 to 1.5 GPa for  $n$  between 8 and 9, that is, to below the value of around 1.8 GPa observed for PA610 (Figure 6c).

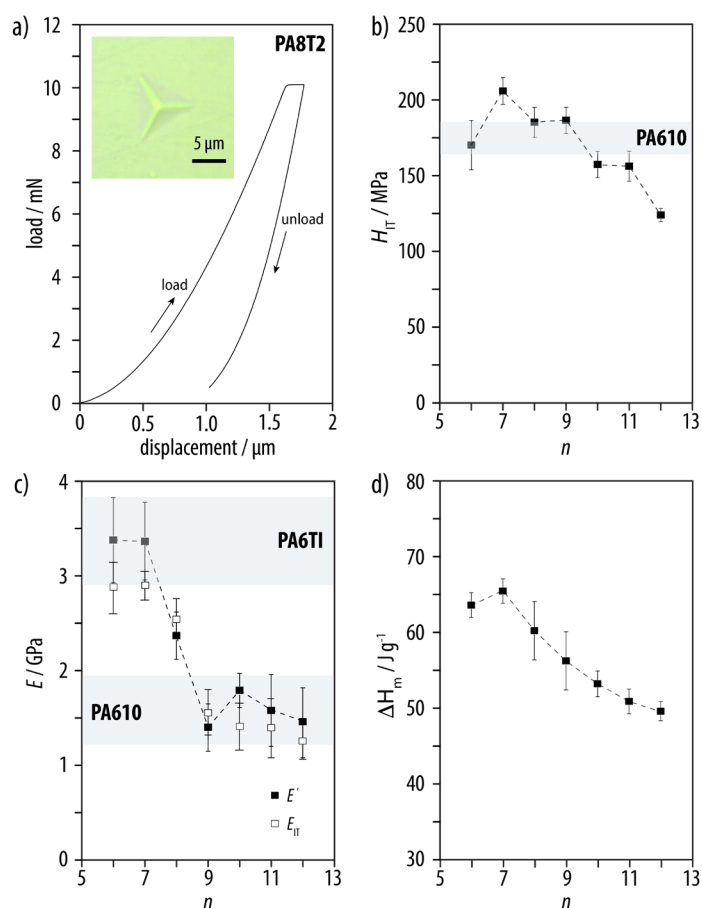


**Figure 6.** a) Typical load-displacement curves with the residual imprint (inset) from nanoindentation measurements on the **PA $n$ T2** films. b) Instrumented hardness ( $H_{IT}$ ) and c) elastic modulus from the indentation measurements,  $E_{IT}$ , and from dynamic mechanical analysis,  $E'$ , of **PA $n$ T2** as a function of  $n$ . For comparison, the moduli of industrial-grade PA610 and PA6TI were shown as a broad range, representing the results obtained from nanoindentation and DMA. d) Melting enthalpy of the specimens hot-pressed at their melting maxima.

The average tensile storage moduli,  $E'$ , determined for comparison by DMA measurements on the same **PA $n$ T2** films showed a similar trend, decreasing gradually from 3.4 to 1.5 GPa for  $n$  between 6 and 12 (Figure 6c), consistent with a reported decrease in the tensile modulus from 2.1 GPa to 1.7 GPa as  $n$  is increased from 6 to 10 in PA $n$ 10.<sup>45</sup> The bithiophene-containing polyamides were hence confirmed to show similar effective strengths and stiffnesses to representative industrial-grade engineering polymers such as PA610 and PA6TI.<sup>46</sup>

### *Optoelectronic Properties*

UV-vis absorption spectroscopy of **PA6T2** and the model compound **T2a** in HFIP showed an absorption band with a maximum at 317 nm and a shoulder at around 340 nm (Figure 7a, solid lines). Thin films of **PA6T2** and the model compound **T2a** spin-coated onto quartz substrates exhibited similar absorptions with slightly red-shifted absorption maxima at 323 and 321 nm, respectively, and shoulders at around 360 nm (Figure 7a, dashed lines). **PA6T2** also underwent photo-bleaching in HFIP when irradiated at 317 nm (Supplementary Figure S7), indicating that the photo-excited state is prone irreversible electron transfer and oxidation reactions.

Pulse-radiolysis time-resolved microwave conductivity (PR-TRMC) was used as an initial probe of the charge transport properties. PR-TRMC measurements on specimens of the polyamides **PA $n$ T2** for  $n = 6$  and 12, as well as the model compound **T2a** at room temperature in the range of 28 to 38 GHz with pulse widths of 2–20 ns (Figure 7b) resulted in mobilities,  $\mu$ , of 0.044 cm<sup>2</sup> V<sup>-1</sup> s<sup>-1</sup> (**T2a**), 0.017 cm<sup>2</sup> V<sup>-1</sup> s<sup>-1</sup> (**PA6T2**) and 0.018 cm<sup>2</sup> V<sup>-1</sup> s<sup>-1</sup> (**PA12T2**). These mobilities are around one order of magnitude higher than the highest values of 0.005 cm<sup>2</sup> V<sup>-1</sup> s<sup>-1</sup> reported for other bithiophene-based systems,<sup>47</sup> and close to those in crystalline quaterthiophene and sexithiophene-based systems.<sup>48–51</sup> This is considered to reflect the beneficial effect of hydrogen bonded substituents on the packing of  $\pi$ -conjugated systems and hence the charge transport properties of the materials.<sup>52</sup>

Despite the promising charge carrier mobilities, field-effect transistors in either top-contact or bottom-contact configuration showed no detectable currents. We attribute this observation to the large HOMO-LUMO gap (4.6 eV) and the irreversible electron transfer reactions of bithiophene systems owing to the high-lying LUMO level (-1 eV) (Supplementary Figure S8). The energetic mismatch of the HOMO and LUMO levels with the gold source/drain electrodes may also render the charge carrier injection energetically unfavorable.

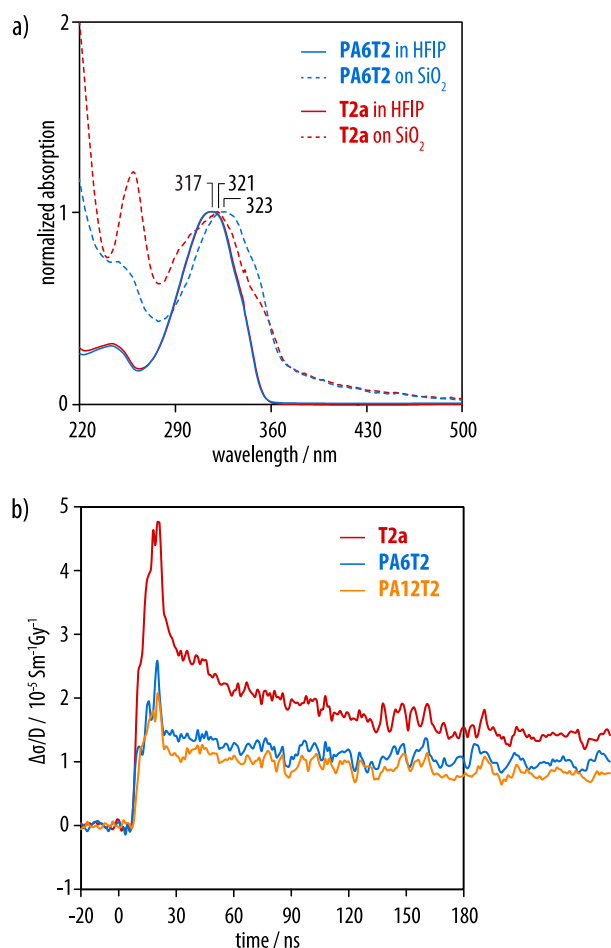


**Figure 7.** a) Normalized UV-vis absorption spectra of **PA6T2** compared with those of the model compound **T2a** from solutions (solid lines) and spin-coated thin films on a quartz substrate (dashed lines). b) Transient change in conductivity of **T2a**, **PA6T2** and **PA12T2** on irradiation with a 10 ns electron pulse normalized by the irradiation dose, D.

## Conclusions

We prepared a series of melt-processable semicrystalline bithiophene-containing polyamides by solution-phase polycondensation under Yamazaki-Higashi conditions. The crystal structures of these polyamides were characterized by a close, parallel-displaced  $\pi$ - $\pi$  stacked arrangement unlike many existing oligothiophenes but similar to that observed in the model compound bithiophene butanamide **T2a**. As a result, PR-TRMC measurements demonstrated charge carrier mobilities that were an order of magnitude greater than in their low molar mass analogues. The morphologies obtained on solidification from melt were similar to those of typical engineering semicrystalline polyamides, consisting of spherulitic agglomerates of interconnected stacked-crystalline lamellae. It follows that the resulting hardnesses and elastic moduli were also similar to those of engineering semicrystalline polyamides. Bithiophene-containing polyamides may therefore represent a step towards polyamide-

based semiconductors, with a synergistic interplay of interchain hydrogen bonding and  $\pi$ - $\pi$  stacking rendering them suitable for applications in which both mechanical and optoelectronic properties play an important role.

## Acknowledgments

The authors gratefully acknowledge funding from the *Schweizerischer Nationalfonds* (SNF grants 200020-144417 and 200020-162774). The research leading to these results at Delft University of Technology has received funding from the European Research Council Horizon 2020 ERC Grant Agreement no. 648433.

## References

- (1) Root, S. E.; Savagatrup, S.; Printz, A. D.; Rodriguez, D.; Lipomi, D. J. Mechanical Properties of Organic Semiconductors for Stretchable, Highly Flexible, and Mechanically Robust Electronics. *Chem. Rev.* **2017**, *117* (9), 6467–6499. <https://doi.org/10.1021/acs.chemrev.7b00003>.
- (2) Heeger, A. J. Nobel Lecture: Semiconducting and Metallic Polymers: The Fourth Generation of Polymeric Materials. *Rev. Mod. Phys.* **2001**, *73* (3), 681–700. <https://doi.org/10.1103/RevModPhys.73.681>.
- (3) Noriega, R.; Rivnay, J.; Vandewal, K.; Koch, F. P. V.; Stingelin, N.; Smith, P.; Toney, M. F.; Salleo, A. A General Relationship between Disorder, Aggregation and Charge Transport in Conjugated Polymers. *Nat. Mater.* **2013**, *12* (11), 1038–1044. <https://doi.org/10.1038/nmat3722>.
- (4) Rivnay, J.; Mannsfeld, S. C. B.; Miller, C. E.; Salleo, A.; Toney, M. F. Quantitative Determination of Organic Semiconductor Microstructure from the Molecular to Device Scale. *Chem. Rev.* **2012**, *112* (10), 5488–5519. <https://doi.org/10.1021/cr3001109>.
- (5) Koch, F. P. V.; Rivnay, J.; Foster, S.; Müller, C.; Downing, J. M.; Buchaca-Domingo, E.; Westacott, P.; Yu, L.; Yuan, M.; Baklar, M.; et al. The Impact of Molecular Weight on Microstructure and Charge Transport in Semicrystalline Polymer Semiconductors–Poly(3-Hexylthiophene), a Model Study. *Prog. Polym. Sci.* **2013**, *38* (12), 1978–1989.
- (6) Sirringhaus Henning. 25th Anniversary Article: Organic Field-Effect Transistors: The Path Beyond Amorphous Silicon. *Adv. Mater.* **2014**, *26* (9), 1319–1335. <https://doi.org/10.1002/adma.201304346>.
- (7) Grozema, F. C.; Siebbeles, L. D. A. Mechanism of Charge Transport in Self-Organizing Organic Materials. *Int. Rev. Phys. Chem.* **2008**, *27* (1), 87–138. <https://doi.org/10.1080/01442350701782776>.
- (8) Ashizawa, M.; Zheng, Y.; Tran, H.; Bao, Z. Intrinsically Stretchable Conjugated Polymer Semiconductors in Field Effect Transistors. *Prog. Polym. Sci.* **2019**, 101181. <https://doi.org/10.1016/j.progpolymsci.2019.101181>.
- (9) McCullough, R. D.; Tristram-Nagle, S.; Williams, S. P.; Lowe, R. D.; Jayaraman, M. Self-Orienting Head-to-Tail Poly(3-Alkylthiophenes): New Insights on Structure-Property Relationships in Conducting Polymers. *J. Am. Chem. Soc.* **1993**, *115* (11), 4910–4911. <https://doi.org/10.1021/ja00064a070>.
- (10) Sirringhaus, H.; Brown, P. J.; Friend, R. H.; Nielsen, M. M.; Bechgaard, K.; Langeveld-Voss, B.; Spiering, A.; Janssen, R. A.; Meijer, E. W.; Herwig, P. Two-Dimensional Charge Transport in Self-Organized, High-Mobility Conjugated Polymers. *Nature* **1999**, *401* (6754), 685–688.
- (11) Wang, S.; Fabiano, S.; Himmelberger, S.; Puzinas, S.; Crispin, X.; Salleo, A.; Berggren, M. Experimental Evidence That Short-Range Intermolecular Aggregation Is Sufficient for Efficient Charge Transport in Conjugated Polymers. *Proc. Natl. Acad. Sci.* **2015**, *112* (34), 10599–10604. <https://doi.org/10.1073/pnas.1501381112>.
- (12) Lee, S. S.; Phillips, P. J. Melt Crystallized Polyamide 6.6 and Its Copolymers, Part I. Melting Point – Lamellar Thickness Relations in the Homopolymer. *Eur. Polym. J.* **2007**, *43* (5), 1933–1951. <https://doi.org/10.1016/j.eurpolymj.2007.01.051>.
- (13) Candau, N.; Galland, S.; Cretenoud, J.; Balog, S.; Michaud, V.; chenai, J.-M.; Lame, O.; Plummer, C. J. G.; Frauenrath, H. High-Performance Polyamides with Engineered Disorder Show Exceptional Ductility. *Be Submitt.*
- (14) Marchildon Keith. Polyamides – Still Strong After Seventy Years. *Macromol. React. Eng.* **2011**, *5* (1), 22–54. <https://doi.org/10.1002/mren.201000017>.
- (15) Jalal Uddin, A.; Ohkoshi, Y.; Gotoh, Y.; Nagura, M.; Endo, R.; Hara, T. Melt Spinning and Laser-Heated Drawing of a New Semiaromatic Polyamide, PA9-T Fiber. *J. Polym. Sci. Part B Polym. Phys.* **2004**, *42* (3), 433–444. <https://doi.org/10.1002/polb.10710>.

- (16) Cretenoud Julien; Galland Sylvain; Plummer Christopher J. G.; Michaud Véronique; Bayer Andreas; Lamberts Nikolai; Hoffmann Botho; Frauenrath Holger. High-temperature Copolyamides Obtained by the Efficient Transamidation of Crystalline–Crystalline Polyamide Blends. *J. Appl. Polym. Sci.* **2016**, *134* (4). <https://doi.org/10.1002/app.44349>.
- (17) Muguruma, H.; Yudasaka, M.; Hotta, S. Vapor Polymerization Deposition of New Polyamide Thin Films Having Oligothiophene Segments in the Main Chain. *Thin Solid Films* **1999**, *339*, 120–122.
- (18) Muguruma, H.; Matsumura, K.; Hotta, S. Molecular Orientation of Oligothiophene-Based Polyamide Thin Films Fabricated by Vapor Deposition Polymerization. *Thin Solid Films* **2002**, *405*, 77–80.
- (19) Bauer, S.; Kaltenbrunner, M. Semiconductors That Stretch and Heal. *Nature* **2016**, *539* (7629), 365–367. <https://doi.org/10.1038/539365a>.
- (20) Głowacki Eric Daniel; Irimia-Vladu Mihai; Kaltenbrunner Martin; Gsiorowski Jacek; White Matthew S.; Monkowius Uwe; Romanazzi Giuseppe; Suranna Gian Paolo; Mastroianni Piero; Sekitani Tsuyoshi; et al. Hydrogen-Bonded Semiconducting Pigments for Air-Stable Field-Effect Transistors. *Adv. Mater.* **2012**, *25* (11), 1563–1569. <https://doi.org/10.1002/adma.201204039>.
- (21) Gsänger Marcel; Oh Joon Hak; Könemann Martin; Höffken Hans Wolfgang; Krause Ana-Maria; Bao Zhenan; Würthner Frank. A Crystal-Engineered Hydrogen-Bonded Octachloroperylene Diimide with a Twisted Core: An N-Channel Organic Semiconductor. *Angew. Chem. Int. Ed.* **2009**, *49* (4), 740–743. <https://doi.org/10.1002/anie.200904215>.
- (22) Zhang Ming-Xing; Zhao Guang-Jiu. Modification of N-Type Organic Semiconductor Performance of Perylene Diimides by Substitution in Different Positions: Two-Dimensional  $\pi$ -Stacking and Hydrogen Bonding. *ChemSusChem* **2012**, *5* (5), 879–887. <https://doi.org/10.1002/cssc.201100510>.
- (23) Liu, H.; Brémond, É.; Prlj, A.; Gonthier, J. F.; Corminboeuf, C. Adjusting the Local Arrangement of  $\pi$ -Stacked Oligothiophenes through Hydrogen Bonds: A Viable Route to Promote Charge Transfer. *J. Phys. Chem. Lett.* **2014**, *5* (13), 2320–2324. <https://doi.org/10.1021/jz501078s>.
- (24) Özen, B.; Tirani, F. F.; Scopelliti, R.; Frauenrath, H. Structure-Property Relationships in Bithiophenes with Hydrogen-Bonded Substituents. *Be Submitt.*
- (25) Rigaku Oxford Diffraction. 2015.
- (26) Sheldrick, G. M. SHELXT – Integrated Space-Group and Crystal-Structure Determination. *Acta Crystallogr. Sect. Found. Adv.* **2015**, *71* (1), 3–8. <https://doi.org/10.1107/S2053273314026370>.
- (27) Sheldrick, G. M. Crystal Structure Refinement with SHELXL. *Acta Crystallogr. Sect. C Struct. Chem.* **2015**, *71* (1), 3–8. <https://doi.org/10.1107/S2053229614024218>.
- (28) Strobl, G. R.; Schneider, M. Direct Evaluation of the Electron Density Correlation Function of Partially Crystalline Polymers. *J. Polym. Sci. Polym. Phys. Ed.* **1980**, *18* (6), 1343–1359. <https://doi.org/10.1002/pol.1980.180180614>.
- (29) Mayo, S. L.; Olafson, B. D.; Goddard, W. A. DREIDING: A Generic Force Field for Molecular Simulations. *J. Phys. Chem.* **1990**, *94* (26), 8897–8909. <https://doi.org/10.1021/j100389a010>.
- (30) Oliver, W. C.; Pharr, G. M. An Improved Technique for Determining Hardness and Elastic Modulus Using Load and Displacement Sensing Indentation Experiments. *J. Mater. Res.* **1992**, *7* (06), 1564–1583. <https://doi.org/10.1557/JMR.1992.1564>.
- (31) Infelta, P. P.; de Haas, M. P.; Warman, J. M. The Study of the Transient Conductivity of Pulse Irradiated Dielectric Liquids on a Nanosecond Timescale Using Microwaves. *Radiat. Phys. Chem.* **1977**, *10* (5), 353–365. [https://doi.org/10.1016/0146-5724\(77\)90044-9](https://doi.org/10.1016/0146-5724(77)90044-9).
- (32) Warman, J. M.; de Haas, M. P.; Dicker, G.; Grozema, F. C.; Piris, J.; Debije, M. G. Charge Mobilities in Organic Semiconducting Materials Determined by Pulse-Radiolysis Time-Resolved Microwave Conductivity:  $\pi$ -Bond-Conjugated Polymers versus  $\pi$ - $\pi$ -Stacked Discotics. *Chem. Mater.* **2004**, *16* (23), 4600–4609. <https://doi.org/10.1021/cm049577w>.
- (33) Yamazaki, N.; Higashi, F.; Kawabata, J. Studies on Reactions of the N-Phosphonium Salts of Pyridines. XI. Preparation of Polypeptides and Polyamides by Means of Triaryl Phosphites in Pyridine. *J. Polym. Sci. Polym. Chem. Ed.* **1974**, *12* (9), 2149–2154. <https://doi.org/10.1002/pol.1974.170120935>.
- (34) Yamazaki, N.; Matsumoto, M.; Higashi, F. Studies on Reactions of the N-Phosphonium Salts of Pyridines. XIV. Wholly Aromatic Polyamides by the Direct Polycondensation Reaction by Using Phosphites in the Presence of Metal Salts. *J. Polym. Sci. Polym. Chem. Ed.* **1975**, *13* (6), 1373–1380. <https://doi.org/10.1002/pol.1975.170130609>.
- (35) Yamazaki, N.; Higashi, F. Studies on Reactions of N-Phosphonium Salts of Pyridines. VIII. Preparation of Polyamides by Means of Diphenyl Phosphite in Pyridine. *J. Polym. Sci. Polym. Lett. Ed.* **1974**, *12* (4), 185–191. <https://doi.org/10.1002/pol.1974.130120402>.
- (36) Coffman, D. D.; Berchet, G. J.; Peterson, W. R.; Spanagel, E. W. Polymeric Amides from Diamines and Dibasic Acids. *J. Polym. Sci.* **1947**, *2* (3), 306–313. <https://doi.org/10.1002/pol.1947.120020308>.
- (37) Kinoshita, Y. An Investigation of the Structures of Polyamide Series. *Makromol. Chem.* **33** (1), 1–20. <https://doi.org/10.1002/macp.1959.020330101>.
- (38) Murthy N. Sanjeeva. Hydrogen Bonding, Mobility, and Structural Transitions in Aliphatic Polyamides. *J. Polym. Sci. Part B Polym. Phys.* **2006**, *44* (13), 1763–1782. <https://doi.org/10.1002/polb.20833>.
- (39) Li, Y.; Zhu, X.; Tian, G.; Yan, D.; Zhou, E. Multiple Melting Endotherms in Melt-Crystallized Nylon 10,12. *Polym. Int.* **2001**, *50* (6), 677–682.
- (40) Skrovanek, D. J.; Painter, P. C.; Coleman, M. M. Hydrogen Bonding in Polymers. 2. Infrared Temperature Studies of Nylon 11. *Macromolecules* **1986**, *19*, 699–705.
- (41) Morales-Gómez, L.; Soto, D.; Franco, L.; Puiggalí, J. Brill Transition and Melt Crystallization of Nylon 56: An Odd–Even Polyamide with Two Hydrogen-Bonding Directions. *Polymer* **2010**, *51* (24), 5788–5798. <https://doi.org/10.1016/j.polymer.2010.09.074>.
- (42) Bunn, C. W.; Garner, E. V. The Crystal Structures of Two Polyamides ('Nylons'). *Proc. R. Soc. Math. Phys. Eng. Sci.* **1947**, *189* (1016), 39–68. <https://doi.org/10.1098/rspa.1947.0028>.

- (43) Fereydoon, M.; Tabatabaei, S. H.; Aji, A. Rheological, Crystal Structure, Barrier, and Mechanical Properties of PA6 and MXD6 Nanocomposite Films. *Polym. Eng. Sci.* **2014**, *54* (11), 2617–2631. <https://doi.org/10.1002/pen.23813>.
- (44) Doudou, B. B.; Dargent, E.; Grenet, J. Relationship between Draw Ratio and Strain-Induced Crystallinity in Uniaxially Hot-Drawn PET MXD6 Films. *J. Plast. Film Sheeting* **2005**, *21* (3), 233–251. <https://doi.org/10.1177/8756087905058248>.
- (45) Biron, M. *Industrial Applications of Renewable Plastics: Environmental, Technological, and Economic Advances*; Elsevier Science, 2016.
- (46) Kohan, M. I.; Mestemacher, S. A.; Pagilagan, R. U.; Redmond, K. Polyamides. In *Ullmann's Encyclopedia of Industrial Chemistry*; Wiley-VCH Verlag GmbH & Co. KGaA, Ed.; Wiley-VCH Verlag GmbH & Co. KGaA: Weinheim, Germany, 2003. [https://doi.org/10.1002/14356007.a21\\_179.pub2](https://doi.org/10.1002/14356007.a21_179.pub2).
- (47) Schoonbeek, F. S.; van Esch, J. H.; Wegewijs, B.; Rep, D. B. A.; de Haas, M. P.; Klapwijk, T. M.; Kellogg, R. M.; Feringa, B. L. Efficient Intermolecular Charge Transport in Self-Assembled Fibers of Mono- and Bithiophene Bisurea Compounds. *Angew. Chem. Int. Ed.* **1999**, *38* (10), 1393–1397.
- (48) de Haas, M.; van der Laan, G.; Wegewijs, B.; de Leeuw, D.; Bäuerle, P.; Rep, D. B. A.; Fichou, D. Mobile Charge Carriers in Pulse-Irradiated Poly- and Oligothiophenes. *Synth. Met.* **1999**, *101*, 524–525.
- (49) Grozema, F. C.; Wegewijs, B. R.; de Haas, M.; Siebbeles, L. D. A.; de Leeuw, D.; Wilson, R.; Sirringhaus, H. Frequency Dependence of the Charge Carrier Mobility in DH4T. *Synth. Met.* **2001**, *119*, 463–464.
- (50) Wegewijs, B.; de Haas, M.; de Leeuw, D.; Wilson, R.; Sirringhaus, H. Charge Carrier Mobilities in Mesomorphic  $\alpha,\omega$ -Dihexylquaterthiophene: A Comparative Microwave Conductivity and Thin Film Transistor Study. *Synth. Met.* **1999**, *101*, 534–535.
- (51) Pratihar, P.; Ghosh, S.; Stepanenko, V.; Patwardhan, S.; Grozema, F. C.; Siebbeles, L. D. A.; Würthner, F. Self-Assembly and Semiconductivity of an Oligothiophene Supergelator. *Beilstein J. Org. Chem.* **2010**, *6*, 1070–1078. <https://doi.org/10.3762/bjoc.6.122>.
- (52) Gebers, J.; Özen, B.; Hartmann, L.; Schaer, M.; Suárez, S.; Bugnon, P.; Scopelliti, R.; Steinrück, H.-G.; Konovalov, O.; Magerl, A.; et al. Crystal Structure, Thin Film Morphology, and OFET Performance of a Hydrogen-Bonded Quaterthiophene. *submitted* 1–20.

## Table of Contents Figure

Incorporation of bithiophene segments in the polyamides result semiconducting properties, while maintaining mechanical properties of typical engineering polyamides.

